Supplementary Information for

Extreme weather events recorded by daily to hourly resolution biogeochemical proxies of marine Giant Clam shells

Hong Yan*, Chengcheng Liu, Zhisheng An*, Wei Yang*, Yuanjian Yang, Ping Huang, Shican Qiu, Pengchao Zhou, Nanyu Zhao, Haobai Fei, Xiaolin Ma, Ge Shi, John Dodson, Jialong Hao, Kefu Yu, Gangjian Wei, Yanan Yang, Zhangdong Jin, Weijian Zhou

This file includes:

Methods S1 to S6

Texts S1 to S5

Table S1

Figures S1 to S14

References

Methods S1 to S6

(S1) Instrumental data source and Local Tropical Cyclone Index (LTI) definition

The meteorological data in the study area, including surface air temperature, precipitation, wind speed and visibility, were measured automatically in Shanhu and Yongxing weather stations which are about 60 and 90 kilometers away from the North Reef, respectively. The resolution of the meteorological data is 3 hourly. The data of sea surface temperature were from the ECMWF (https://www.ecmwf.int/) with a time resolution of 3 hours. The 3-day averaged sea surface wind vectors at 10 m above the sea with spatial resolution of 25 km are produced by Remote Sensing Systems (http://www.remss.com/). Merged daily chlorophyll-a concentration (Chl-a) data with high-resolution of 4 km from Ocean Colour Climate Change Initiative dataset were produced and distributed by the European Space Agency (http://www.esa-oceancolour-cci.org/).

The tropical cyclone data (6 hours resolution) were from the JTWC (Joint Typhoon Warning Center: http://www.metoc.navy.mil/jtwc/jtwc.html). In order to quantitatively assess the impacts of western Pacific TCs on regional weather/climate conditions and upper ocean environments, a Local TC Index (LTI) is defined. The definition of the LTI index considers both the intensity of TC and the distance of TC center away from the North Reef (sampling site).

$$LTI=1000*M/D$$

M is the maximum wind speed of TC and D is the distance between TC center and the sampling site. The LTI of each selected TC varies with time because the wind speed and distances are variable. The LTI of all TCs in the western Pacific were calculated and the LTI over 10 is considered to have a significant impact on local climate based on the comparison between LTI and local meteorological data.

Based on the LTI calculation, a total of 37 TCs which had significant impacts (LTI >10) on the weather of sampling site North Reef were obtained from January 29, 2012 to December 9, 2013. We number them in chronological order from 1 to 37 and show the number in Figure 2, 3, *SI Appendix, Table S1, Fig. S2, S8, S10 and S11*. Detailed information of these 37 TCs are shown in *SI Appendix, Table S1*. The table

includes the Number, Tropical cyclone ID, Name, Date, Category, Maximum wind velocity of TC, Minimum distance between TC center and North Reef, Maximum LTI, lat/long at Maximum LTI, Duration above LTI>10, Accumulated LTI.

The circles are used to indicate the Category and Distance of the TCs in Figure 2, 3, *SI Appendix, Fig. S2, S8 and S10*. The size of the circle represents the category of TCs. The super typhoon (SuperTY), strong typhoon (STY), typhoon (TY), tropical storm (TS) and tropical depression (TD) are represented by circles of 6, 5, 4, 3 and 2 mm diameter respectively. The color of the circle represents the minimum distance between the TC and the sampling site at North Reef. The distance over 600 km, 300-600 km, 100-300km and below 100 km are represented by red with the transparency 75%, 50%, 25% and 0%. Thus the larger the circle means the stronger the TC and the deeper the red means the closer of the TC to the North Reef.

The winter cold surges are calculated by air temperature data of the Shanhu and Yongxing weather stations. A cold surge event is defined when the temperature drops 2 ℃ relative to the previous 15 days average and the minimum temperature is below 23 ℃. Severn cold surges were identified from January 29, 2012 to December 9, 2013.

(S2) Sample preparation and LSCM analyses

After removing the soft tissue, the center of one side of the shell was cut from its umbo to the ventral margin along the maximum growth axis (Fig. 1 b and c). Then a radial section was cut by using a fixed diamond endless wire saw cutting machine. After the preparation, a radial growth part was mounted in an epoxy resin disk. The length of the sub-sample is 16.8 mm and the inner layer part is 12.6 mm along the growth direction (Fig. 1d). Mounted samples were polished with a polishing sheet with fine diamond grains embedded on the surface. Final polishing was done with a 0.5-μm diamond suspension. Images at 10x magnification of the polished shell slab were produced on a Nikon A1 Laser Scanning Confocal Microscope (LSCM) at the State Key Laboratory for Manufacturing Systems Engineering, Xi'an Jiaotong University. Laser excitation wavelengths of 488 nm triggered auto-fluorescence of the fluorescent material incorporated in the calcite lattice with emission detection 500 to

550 nm.

(S3) High resolution NanoSIMS analysis

Measurement of major and trace elements was performed by a CAMECA NanoSIMS 50L (CAMECA, Paris, France). Before the measurement, the polished surface was carbon coated to avoid charging during the analysis. Firstly, the high resolution NanoSIMS analysis was performed on the 12.6-mm growth lifetime of the *Tridacna* shell XB10. A Cs+ beam of ~150 pA and ~ 300 nm in diameter was used, with an accelerating high voltage of 16 kV. Each analysis consists of 25 blocks of 10 cycles with a total integrating time of ~200 seconds by rastering the primary beam over 2x2 μm^2 areas with ~2 μm interval spot by spot. And $^{40}Ca^{16}O$, $^{88}Sr^{16}O$ and $^{56}Fe^{16}O$ were measured simultaneously by the multi-collector system with a mass resolving power (MRP) of ~6000 (10% definition). The data were used to calculate the Sr/Ca and Fe/Ca ratios. Data at 1402-1600 μm were lost due to the breakdown of the NanoSIMS. Secondly, a repeating measurement was performed on the *Tridacna* shell XB10 from 300μm to 600μm using a ~100-150 pA primary beam of $^{16}O^-$ with spatial resolution of ~2x2 μm^2 and 2 μm interval. $^{44}Ca^+$, $^{88}Sr^+$, $^{57}Fe^+$, $^{55}Mn^+$ and $^{138}Ba^+$ ion were measured simultaneously to calculate the Sr/Ca, Fe/Ca, Mn/Ca and Ba/Ca ratios. The results of the two measurements were consistent, showing that this method has good repeatability (*SI Appendix, Fig. S5*).

(S4) Low resolution Sr/Ca analyses by ICP-OES

The carbonate sub-samples of about 50 μg for Sr/Ca analysis were micro-milled along growth increments (The same with the NanoSIMS analyses) with 0.15 mm interval. Each powder subsample was completely dissolved in 2 ml 5% HNO_3, about 1.5 ml of solution was used for the Sr/Ca measurement. The Sr/Ca ratios were determined by an Inductively Coupled Plasma Optical Emission Spectrometer (ICP-OES, spectral lines

Ca: 317.933nm, Sr: 407.711nm). In order to monitor the status of the instrument, we inserted a laboratory mark N1 between every 5 subsamples, the average Sr/Ca value of N1 is 2.305±0.0009 mmol/mol, and the relative standard deviation (RSD) is 0.437%. The low resolution (150μm interval, weekly to monthly) Sr/Ca results showed consistent variations with the NanoSIMS data (*SI Appendix, Fig. S6*).

(S5) Daily resolution chronology

The micro-image derived from the LSCM showed that the shell has clear diurnal growth layers during the 12.6-mm growth life period except the first 1.6mm from the inner edge (Fig. 1e and *SI Appendix, Fig. S3*). The number of the daily layers from the distance of 1.6mm to 12.6mm was counted from the LSCM images by three persons and the total number of the daily growth layers is 587, 591 and 592, respectively. The Sr/Ca ratios show clear daily cycles during the whole 12.6-mm growth lifetime and the total number of the Sr/Ca daily cycles is 680. From the distance of 1.6mm to 12.6mm, the number of the Sr/Ca daily cycles is 590, which is basically consistent with the results from the direct measurement of the daily growth bands using the LSCM images within the range of error, indicating that both the LSCM daily growth bands and the Sr/Ca daily cycles can be used to build the daily resolution age model of the *Tridacna* shell. Based upon the daily growth bands and Sr/Ca daily cycles, together with the collected date (at December 9, 2013), the daily resolution chronology was established for the lifetime of the XB10. The total growth lifetime of the XB10 (0-12.6 mm) was 680 days, from January 29, 2012 to December 9, 2013.

(S6) Establishment of the daily growth rate and variance time series

Two methods were used to calculate the daily growth rate of the shell XB10. First, the daily growth rate was measured directly from the width of each daily growth band because the LSCM micro-image showed that the shell has clear daily growth bands from 1.6mm to 12.6mm. The width between two bright parts is defined as the growth

rate of a day. Three persons repeated the measurements to reduce the subjective effects and produced three time series of daily growth rate (DGR-1, DGR-2, DGR-3 in *SI Appendix, Fig. S7*). Second, the daily growth rate can be also calculated by counting the amount of Sr/Ca data in each Sr/Ca daily cycle, because the NanoSIMS test spacing for each Sr/Ca data is the same at 2-μm. The peaks of Sr/Ca correspond to the bright parts of daily bands (Fig. 1e), thus the width between two Sr/Ca peaks is defined as the growth rate of a day and a daily growth rate time series covered the whole 12.6mm was established (DGR-4). The growth rate profiles derived from two methods are highly correlated with each other and the thickness of each daily layer is about 10-30 μm with a mean of 18.5 μm (*SI Appendix, Fig. S7*). A combined daily growth rate profile (DGR-XB10) was established by the average of the four growth rate time series and is used in the main text (Fig. 2). In order to remove the seasonal variations of the daily growth rate, a daily growth rate variance index (DGRV-XB10) is defined by the [(DGR of one day) - (5 days DGR average)] / (5 days DGR average) (Fig. 2). DGRV indicates the changes of the daily growth rate in one day relative to the average of the most recent 5 days. DGRV less than -0.15 is defined as a significant decrease in daily growth rate and means the daily growth rate decreases by more than 15%.

Texts S1 to S5

(S1) Daily resolution growth rate profile

Based on the clear daily growth layers and Sr/Ca daily cycles, we can readily obtain the daily resolution growth rate profile (DGR-XB10) and growth rate variance index profile (DGRV-XB10) of the *Tridacna* shell XB10 (Fig. 2). The adult *Tridacna* basically does not consume food and the growth of shell mainly depends on the photosynthesis of symbiotic zooxanthellae (*1, 2*). Therefore, the perturbations of climate and weather, which have significant impacts on photosynthesis of symbiotic zooxanthellae, probably have great impacts on the growth rate of *Tridacna* shell. The growth rate profile of XB10 present obvious seasonal cycles, with high/low averaged growth rates in the boreal summer/winter, probably linked to the seasonal variation of the temperature and/or insolation (Fig. 2). In addition to the seasonal variation, the growth rates also show many abrupt changes for certain days, probably linked to the tropical cyclones in summer-autumn and cold surges in winter (see Discussion in the main text).

(S2) Daily to hourly resolution Sr/Ca ratio profile

Measurement of the elemental ratios by NanoSIMS was made at 2-μm intervals and 5 to 15 elemental ratio data was obtained from each 10-30 μm wide daily layer (*3*). The average daily elemental data is 9.26 per day (i.e., 6300/680) and the average time resolution for elements/Ca profiles is about 2.5 hours. The 680 Sr/Ca daily cycles were assigned to each corresponding day from January 29, 2012 to December 9, 2013. The time for the data point of maximum Sr/Ca ratio of each daily cycle was set to 00:00 local time and the time for the data points between the Sr/Ca maxima were assigned using linear interpolation with equal time spans (*4*).

The clear daily cycles observed in Sr/Ca profile of XB10 (Fig. 1e) indicated that the hourly resolution *Tridacna* Sr/Ca ratios probably linked to the difference in weather condition between day and night (temperature, solar radiation, etc.). Many

studies have discussed the climate/weather implication of the Sr/Ca ratios in *Tridacna* shell, but the results remain controversial (*3-7*). Some studies have found that the monthly resolution Sr/Ca of *Tridacna* shell was similar to coral Sr/Ca and was significantly related to temperature changes, so it can be used as a proxy of sea surface temperature (*4, 8*). However, some other studies have suggested that the daily variation of Sr/Ca in *Tridacna* shell was mainly controlled by insolation variations and should thus be used as a proxy of insolation (*3*). Recent culture experiments found that both the temperature and insolation contributed to the daily variation of Sr/Ca in *Tridacna* shell (*6*). More controlled culture experiments are still needed to investigate how Sr/Ca ratios in *Tridacna* shell responds to temperature and/or insolation changes before using the *Tridacna* daily Sr/Ca ratio to reconstruct past WEEs.

(S3) Daily to hourly resolution profiles of Fe/Ca, Ba/Ca and Mn/Ca ratios

Fe/Ca profile of XB10 reveals some pulsed peaks (Fig. 2 and Fig. 3), and shares similar variations with Ba/Ca and Mn/Ca ratios (*SI Appendix, Fig. S5*), suggesting that the peaks of Fe/Ca are probably caused by the increased trace nutrients in ambient seawater (*7, 9, 10*). Vertical distribution of oceanic trace nutrients, such as Fe, Ba and Mn, is similar to that of nutrients, with an increased concentration from surface to the subsurface seawater (*10, 11*). Thus, enhanced vertical mixing, Ekman pumping (e.g., upwelling), and so on, which could bring Fe-, Ba- and Mn-riched subsurface seawater to the surface (*10-14*), would result in abrupt increases of these elements in the surface seawater and peaks of Fe/Ca, Ba/Ca and Mn/Ca ratios in the daily layer of the *Tridacna* shell. Therefore, the pulsed peaks in Fe/Ca, Ba/Ca and Mn/Ca ratios of *Tridacna* shell have the potential to trace the abrupt increase of nutrient elements in surface seawater related to the enhanced vertical mixing (usually caused by high wind stress) and upwelling on the daily to hourly timescale.

(S4) Daily to hourly resolution fluorescence intensity profile

Fluorescence intensity of the *Tridacna* shell XB10 derived from the micro-images of LSCM presented clear daily bands (Fig. 1 and *SI Appendix, Fig. S3*). The fluorescence intensity usually reflects the content of the organic matter in the marine biological carbonate (*15-17*). *Tridacna* shells calcification rate was suggested to be higher during the daytime associated with high photosynthetic activity of symbiotic algae (*3, 6*). This pattern presumably regulates the fluorescent material variations in the shell linked to the diurnal insolation/temperature cycles and growth rates. In addition to the daily bands, the fluorescence intensity of the *Tridacna* shell XB10 also presented some striking bright stripes (Fig. 1f and *SI Appendix, Fig. S9*), probably reflecting the abrupt changes of the organic matter in the *Tridacna* shells. Previous studies on corals have shown that the abrupt increase of fluorescence intensity in marine biological carbonate was mainly modulated by the concentration of organic matter in seawater, which was probably related to the phytoplankton bloom/marine primary production outbreak and river input caused by floods (*15, 17*). Thus in addition to resolving daily time scale, the high resolution fluorescence intensity of the *Tridacna* shell also has the potential to be used as the proxy of phytoplankton bloom/ marine primary production outbreak and/or nearshore floods.

(S5) Uncertainties and challenges

Although the pulsed changes in the ultra-high-resolution biological and geochemical records from the *Tridacna* shell, including the daily growth rate, Fe/Ca ratios and fluorescence intensity, clearly recorded the activities of past WEEs, such as the TCs, marine phytoplankton bloom events and cold surges, there are still a bit uncertainties and challenges as followings:

Firstly, it is difficult to relate the present short "paleoweather" records to the underlying longer-term background climate. Short-term record is easy to be fallen entirely within an El Nino or a La Nina phase (2~7-year periodic variations). However,

we only have two-year length records in this study because the large living *Tridacna* are largely absent from North Reef now due to overfishing in recent decades. Nevertheless, we still got some year to year differences in proxy records related to different typhoon weather conditions. We are searching for larger living samples from North Reef for future work. If we can collect large living samples, we can produce longer records (>2 years) to cover different El Nino or La Nina phases. For example, we have collected some large living *Tridacna gigas* samples from the Yongshu Reef, southern SCS (*SI Appendix, Fig. S14*). We are working on one of the shells named MD3. MD3 has a life span of about 23 years with clear daily growth layers. However, southern SCS does not locate in the core occurring area of the western Pacific Tropical cyclones and we are using the daily growth rate of this shell to detect the MJO (Intraseasonal Oscillations) activity. On the other hand, the large fossil and sub-fossil *Tridacna* samples can be found in North Reef and we have collected over 1000 samples, each over 30 years old (see some information in *SI Appendix, Fig. S12*). We plan to get longer paleo-records based on these fossil and sub-fossil *Tridacna* samples after the modern calibration in this paper.

Secondly, it is hard to gauge which proxy parameter we derived is more suitable, or more effective. Therefore, we are trying to use a combined indicator to reconstruct the tropical cyclones, including how to use statistical methods to quickly and quantitatively reconstruct the frequency and intensity of tropical cyclones, and have achieved some preliminary results. However, the current *Tridacna* proxy data (only two years) is not enough to get a statistically significant result. We will focus on this issue in the next study using *Tridacna* shells with a long lifespan. Meanwhile, we are also trying to use a machine learning method to identify and reconstruct the TC activities from the *Tridacna* proxy records.

Thirdly, very rarely weak tropical cyclones occurred in late autumn or even in early winter (e.g., No.1 TC in *SI Appendix, Table S1*), which may mix with cold extremes (see Fig. 4). So it is needed to give a way to tell them (cyclones, or cold extremes) apart.

As shown in Fig. 2 and *SI Appendix, Fig. S2*, most of the tropical cyclones, especially strong tropical cyclones, occurred during the summer-autumn periods, while nearly all the cold surges happened during winter. Therefore, the reconstructed TC activities in summer-autumn period can basically be used to represent the TC activities throughout the year.

The reconstruction of winter cold surges might be affected by some rarely weak tropical cyclones (e.g., tropical depression) during winter, but the results of proxy records in response to TCs and cold surges are quite different. The growth rates have similar responses to winter TCs and cold surges, but the responses of Fe/Ca to cold surges are obviously weaker than that of TCs, which could help us distinguish the winter TCs and cold surges. However, the current *Tridacna* record only contains seven cold surges over two years, it is difficult to use statistical methods to separate winter TCs and cold surges. Hopefully we can solve this problem when we derive a longer-term record in winter in our next study.

Table S1

Number	ID	Name	Date	Category	Maximum wind velocity (km/h)	Minimum distance from North Reef (km)	Max. LTI	Lat/Lon at max. LTI	Duration above LTI>10	Accumulated LTI
1	1201	Nameless	2012021700~ 2012022100	TD	46.3	749.88	33.34	10.4°N, 112.3°E	2012021700~ 2012022100	462.22
2	1202	Pakhar	2012032718~ 2012040118	TS	111.12	812.75	72.62	9.7°N,1 10.8°E	2012032718~ 2012040118	1382.07
3	1204	Mawar	2012053100~ 2012060606	superTY	194.46	1340.84	64.81	21.6°N, 126.2°E	2012053106~ 2012060606	2251.27
4	1206	Talim	2012061700~ 2012062012	TS	92.6	167.10	154.90	18.8°N, 111.9°E	2012061700~ 2012062012	1525.80
5	1207	Doksuri	2012062512~ 2012063000	TS	74.08	569.56	70.23	21.9°N, 113.4°E	2012062606~ 2012063000	606.50
6	1209	Vicente	2012072006~ 2012072500	superTY	212.98	449.78	214.74	21.4°N, 113.8°E	2012072006~ 2012072500	3689.62
7	1210	Saola	2012072700~ 2012080312	STY	166.68	1295.62	66.52	24.3°N, 122.0°E	2012072700~ 2012080312	2645.60
8	1212	Haikui	2012080112~ 2012080918	TY	120.38	1587.12	38.12	27.3°N, 123.9°E	2012080312~ 2012080918	1060.48
9	1214	Kai-tak	2012081112~ 2012081800	TY	120.38	370.85	175.27	20.2°N, 112.8°E	2012081218~ 2012081800	3144.85
10	1215	Tembin	2012081812~ 2012083012	superTY	222.24	690.73	137.53	20.9°N, 116.7°E	2012081812~ 2012083012	8345.94
11	1218	Jelawat	2012091900~ 2012100106	superTY	259.28	1389.68	93.55	20.9°N, 124.1°E	2012092006~ 2012093018	6933.38
12	1221	Gaemi	2012093006~ 2012100700	TS	101.86	247.69	102.47	13.9°N,. 113.0°E	2012093006~ 2012100700	2099.92
13	1224	Son-tinh	2012102218~ 2012102900	superTY	194.46	76.95	844.76	16.6°N, 111.0°E	2012102306~ 2012102900	9135.75
14	1225	Nameless	2012111206~ 2012111406	TD	46.3	948.04	26.37	8.6°N,1 12.2°E	2012111206~ 2012111406	185.97
15	1226	Bopha	2012112612~ 2012120906	superTY	259.28	531.41	218.60	15.4°N, 116.1°E	2012112800~ 2012120906	7327.27
16	1227	Wukong	2012122406~ 2012122906	TS	64.82	839.87	29.77	9.8°N,1 13.5°E	2012122412~ 2012122906	435.48
17	1301	Sonamu	2013010100~ 2013010800	TS	74.08	995.54	39.00	7.9°N,1 12.2°E	2013010218~ 2013010800	642.93
18	1302	Shanshan	2013021918~ 2013022306	TD	46.3	1013.17	21.12	6.6°N,1 09.7°E	2013021918~ 2013022306	240.27

19	1305	Bebinca	2013061918~2013062400	TS	64.82	255.93	136.76	19.4°N, 111.4°E	2013061918~2013062400	1051.01
20	1306	Rumbia	2013062712~2013070206	TY	129.64	250.90	239.14	19.1°N, 112.6°E	2013062806~2013070206	2331.89
21	1307	Soulik	2013070600~2013071312	superTY	231.5	1219.25	58.80	24.6°N, 120.8°E	2013070806~2013071312	2929.27
22	1308	Cimaron	2013071418~2013070900	TS	74.08	852.87	46.90	21.3°N, 118.3°E	2013071500~2013071900	484.43
23	1309	Jebi	2013073012~2012080312	TS	111.12	149.22	347.39	17.8°N, 112.8°E	2013073012~2012080312	2621.90
24	1310	Mangkhut	2013080500~2013080806	TS	83.34	155.42	225.20	16.0°N, 110.6°E	2013080500~2013080806	1084.33
25	1311	Utor	2013080806~2013081512	superTY	240.76	316.36	300.29	19.3°N, 113.4°E	2013080906~2013081512	8306.04
26	1312	Trami	2013081600~2013082300	TY	138.9	1145.46	55.08	25.7°N, 119.6°E	2013081600~2013082300	1370.62
27	1313	Nameless	2013081612~2013081812	TD	55.56	1664.33	16.59	28.9°N, 123.7°E	2013081618~2013081900	137.74
28	1314	Kong-rey	2013082500~2013083100	TS	92.6	1280.60	38.76	21.7°N, 122.8°E	2013082500~2013083100	650.21
29	1315	Toraji	2013083112~2013090400	TS	92.6	1352.70	23.86	28.8°N, 123.6°E	2013083112~2013090400	272.59
30	1317	Usagi	2013091603~2013092306	superTY	250.02	723.24	123.61	22.4°N, 116.8°E	2013091618~2013092306	4898.69
31	1320	Wutip	2013092600~2013100100	superTY	185.2	49.30	2028.48	16.7°N, 111.7°E	2013092600~2013100100	20121.70
32	1322	Fitow	2013092918~2013100700	STY	166.68	1463.07	51.83	25.1°N, 125.9°E	2013093012~2013100700	2326.84
33	1324	Nari	2013100812~2013101512	superTY	185.2	144.53	553.52	15.8°N, 111.5°E	2013100900~2013101512	12761.66
34	1329	Krosa	2013102800~2013110418	superTY	194.46	59.50	420.15	17.6°N, 111.3°E	2013102900~2013110418	7138.68
35	1330	Nameless	2013110106~2013112100	TS	64.82	579.02	51.81	11.9°N, 111.2°E	2013110306~2013111412	763.99
36	1331	Haiyan	2013110206~2013111106	superTY	314.84	163.25	551.29	16.5°N, 110.1°E	2013110412~2013111106	10396.07
37	1332	Podul	2013111112~2013111506	TD	55.56	589.24	50.91	11.8°N, 111.5°E	2013111300~2013111506	346.82

Table S1 Detailed information of recorded tropical cyclones. A total of 37 tropical cyclones which had significant impacts (LTI >10) on the weather at the sampling site North Reef from January 29, 2012 to December 9, 2013. We number them in

chronological order from 1 to 37. The table includes the Number, Tropical cyclone ID, Name, Date, Category, Maximum wind velocity of TC, Minimum distance between TC center and North Reef, Maximum LTI, lat/long at Maximum LTI, Duration above LTI>10, accumulated LTI (*SI Appendix, Method S1* for LTI calculation). The Category of the tropical cyclones include the super typhoon (SuperTY), strong typhoon (STY), typhoon (TY), tropical storm (TS) and tropical depression (TD).

Figures S1 to S14

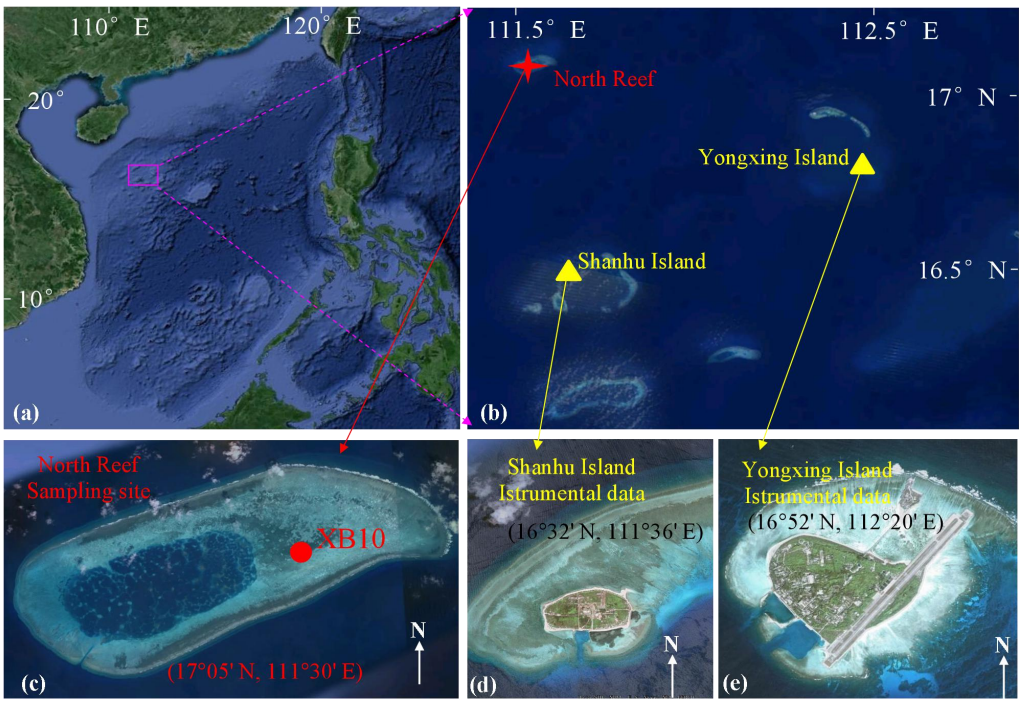

Figure S1 Map of sampling site. (a) Map of the South China Sea; (b) Locations of the North Reef, Shanhu Island and Yongxing Island. (c) Sampling site of the *Tridacna derasa* shell XB10 in North Reef. (d) Shanhu Island weather station, which is about 60 kilometers away from the North Reef. (e) Yongxing Island weather station, which is about 90 kilometers from the North Reef. The meteorological data used in this paper are from these two weather stations.

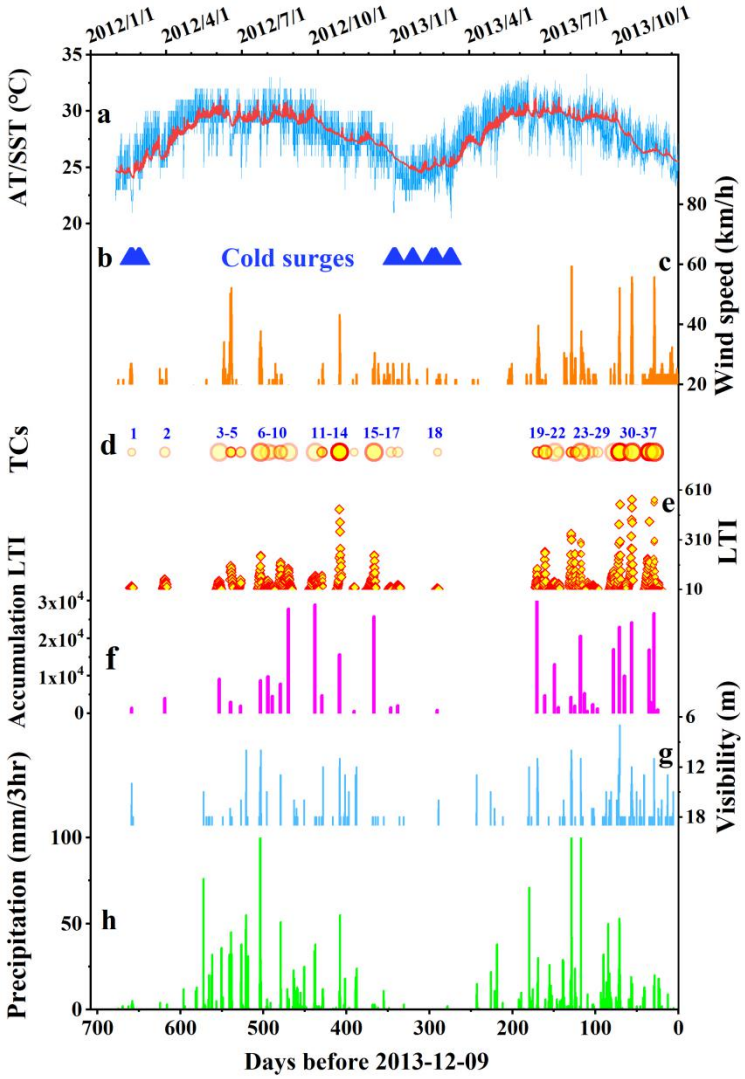

Figure S2 Meteorological data of the sampling site during 2012 and 2013. (a) 3-hour resolution air temperature (AT, blue line) from Shanhu Island weather station and 3-hour sea surface temperature (SST, red line) of North Reef observed by satellite assimilation and reanalysis data (ECMWF: https://www.ecmwf.int/). (b) Winter cold surges (Blue triangle, *SI Appendix, Method S1*). (c) 3-hour resolution wind speed (over 20 km/h) from the Shanhu Island weather station. (d) The circles were used to represent the 37 TCs that have significant impacts on sampling site during the 2012 and 2013. The larger the circle represents the stronger the TC and the deeper the red represents the closer the TC to the sampling site (*SI Appendix, Method S1*). (e) The Local Tropical Cyclone Index (LTI) time series during 2012 and 2013 (*SI Appendix, Method S1*). (f) The accumulated LTI of the each TC during the 2012 and 2013. The detailed information of the 37 TCs is compiled in *SI Appendix, Table S1*. (g) 3-hour resolution visibility from the Shanhu Island weather station. (h) 3-hour resolution precipitation from the Shanhu Island weather station. The tropical cyclones during the summer-autumn periods usually bring strong wind, heavy rainfall, low visibility and decreased temperature to North Reef.

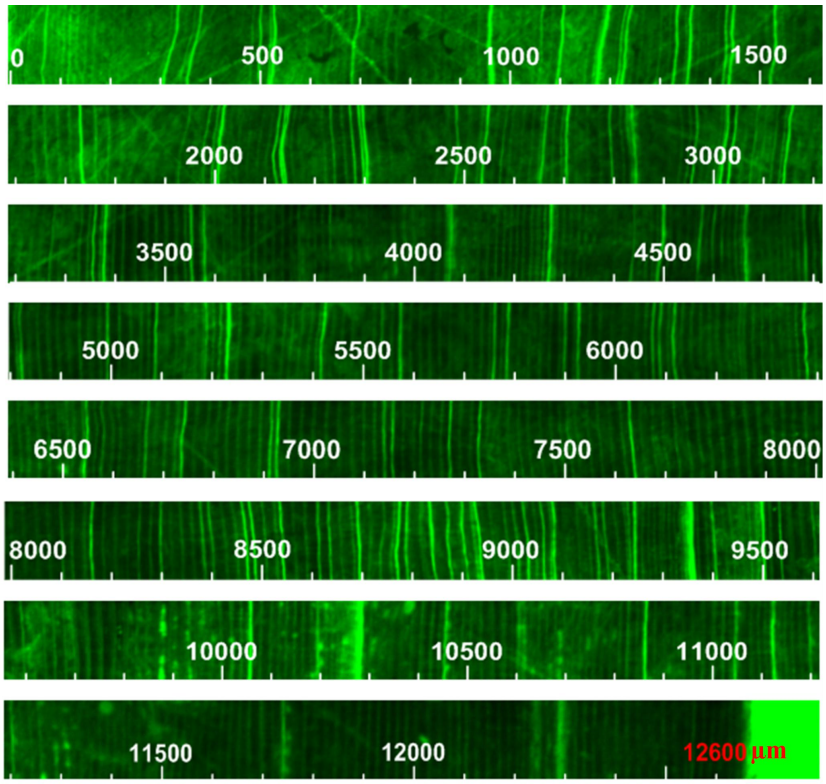

Figure S3 Detailed auto-fluorescence images of the *Tridacna* XB10 obtained by LSCM. The scales indicated the distance from the inner edge.

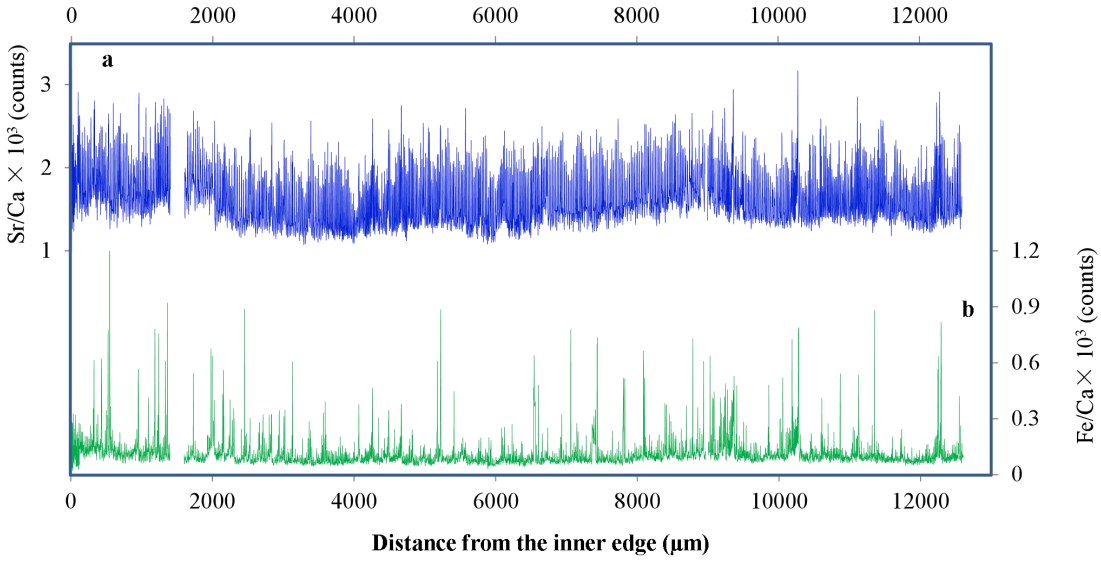

Figure S4 NanoSIMS data of the *Tridacna* sample XB10. (a) Sr/Ca ratios. (b) Fe/Ca ratios. Sr/Ca profile showed clear daily cycles while the Fe/Ca profile presented some pulsed peaks. Data at 1402-1600 μm were lost due to the breakdown of NanoSIMS.

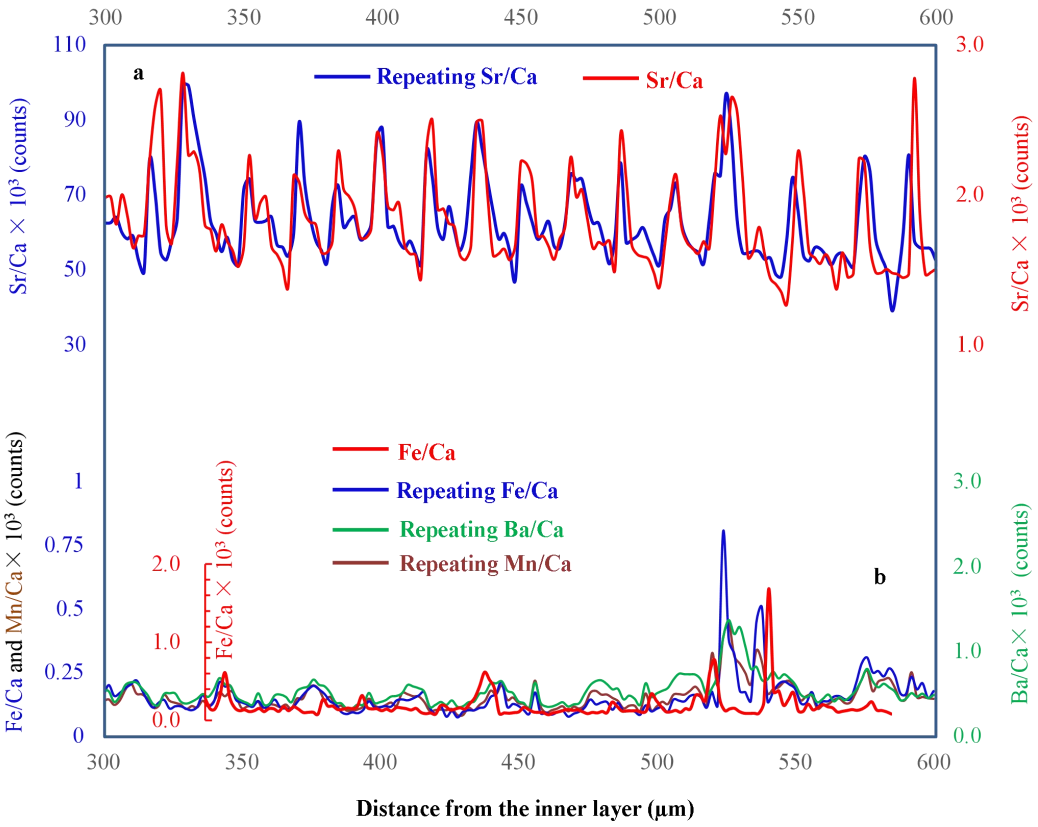

Figure S5 Repeatability of the NanoSIMS data of the *Tridacna* sample XB10. (a) The repeating Sr/Ca values show consistent changes with the Sr/Ca of the original measurement from 300 to 600 μm. (b) The repeating Fe/Ca show consistent changes with the Fe/Ca of the original measurements. Meanwhile, Fe/Ca, Mn/Ca and Ba/Ca showed similar variations. In this study, Cs+ beam is employed for the main test while the $^{16}O^-$ beam is applied for repeating the measurement (*SI Appendix, Method S3*). The ionization efficiency for elements is different under different ion sources, so the absolute values of elements/Ca are different in the two tests. The significant correlation between two tests indicated that both the Cs+ and $^{16}O^-$ beams can produce similar results.

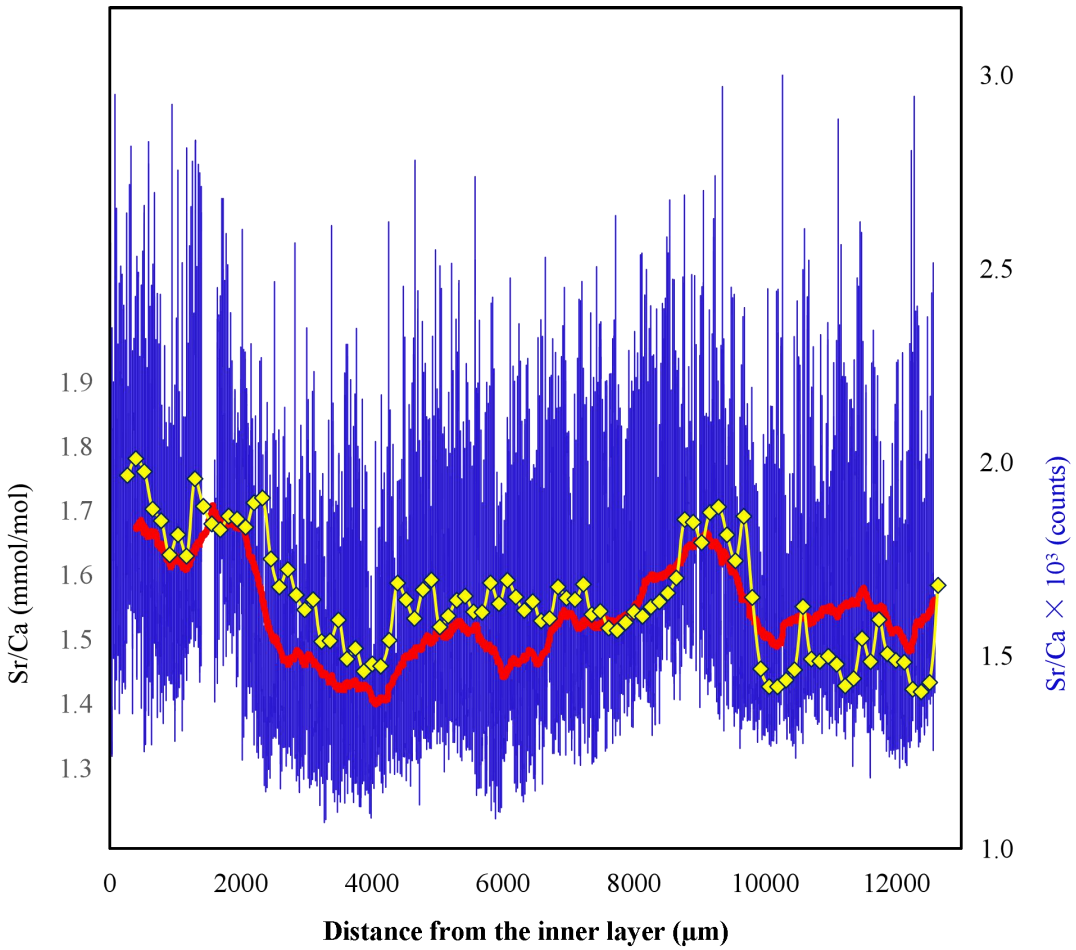

Figure S6 Intercomparison of ultra-high resolution Sr/Ca data (NanoSIMS) and low resolution Sr/Ca data (ICP-OES) of the *Tridacna* sample XB10. The raw data of Sr/Ca determined by NanoSIMS (blue, 2-μm space resolution) and ICP-OES (yellow, 0.15-mm space resolution). 200-point moving average of Sr/Ca ratios determined by NanoSIMS (red).

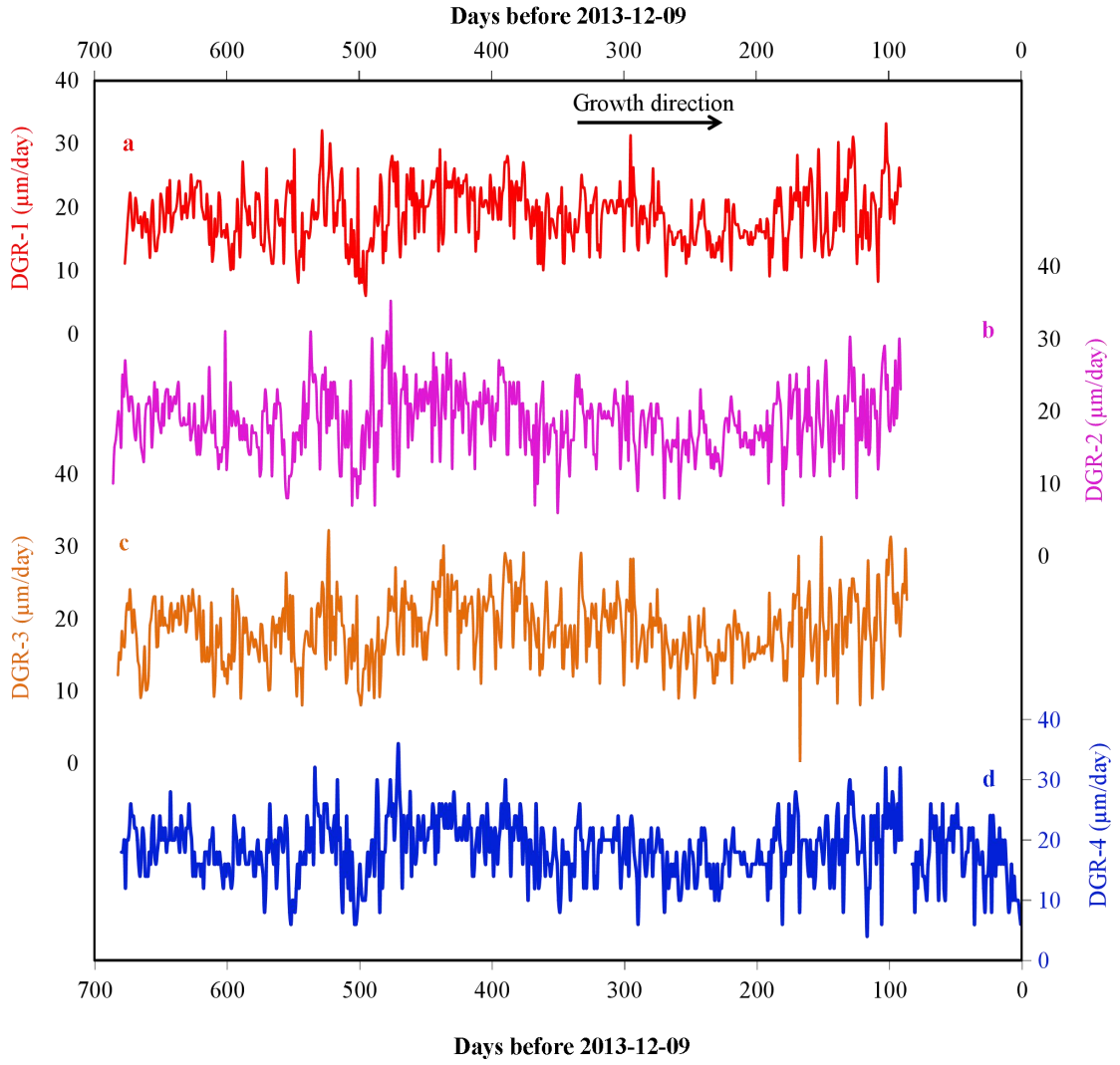

Figure S7 Daily growth rate of the *Tridacna* sample XB10. (a, b and c) The daily growth rate profiles (DGR-1, DGR-2, DGR-3) measured directly from the width of the each daily growth band based on the LSCM auto-fluorescence image (*SI Appendix, Method S6*). (d) Daily growth rate calculated by counting the amount of Sr/Ca data in each Sr/Ca daily cycle (*SI Appendix, Method S6*, DGR-4). A combined daily growth rate profile (DGR-XB10) was established by the average of the four growth rate time series and is used in the main text (*SI Appendix, Method S6*).

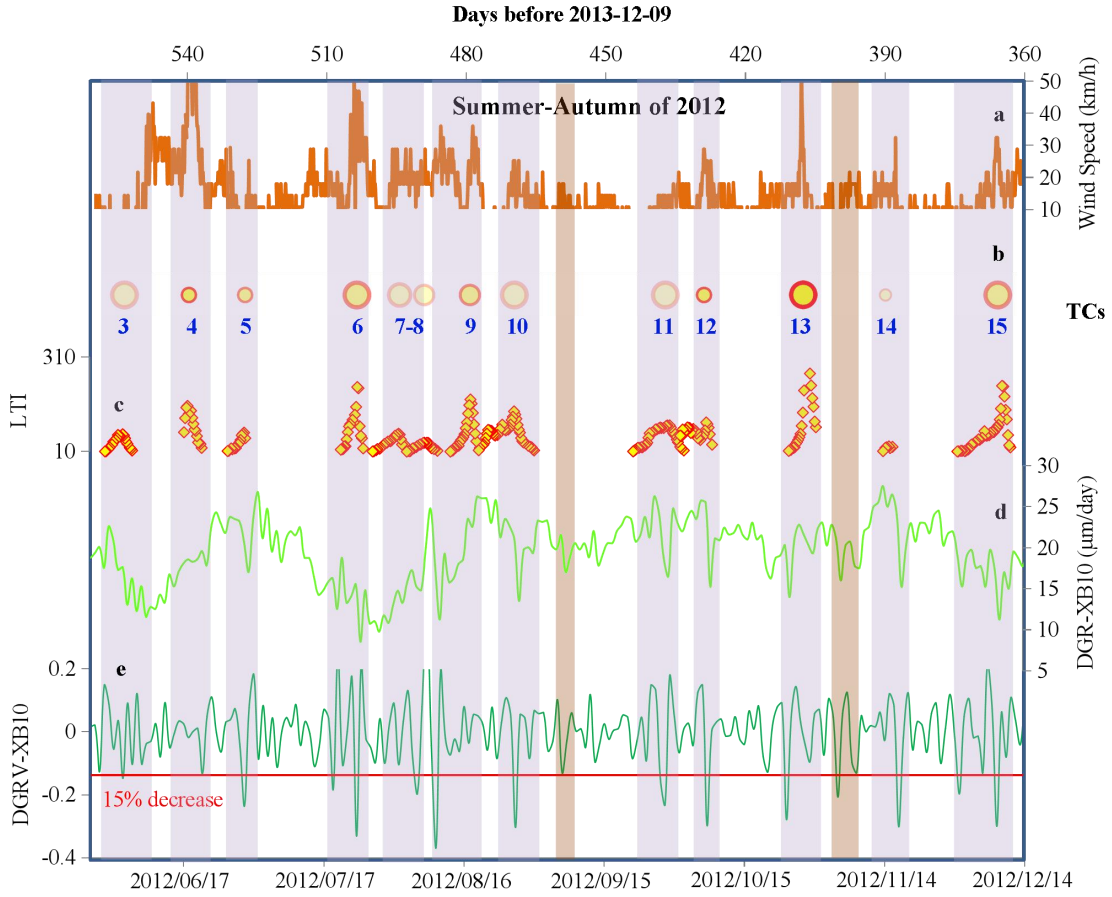

Figure S8-A The matches between the decreased daily growth rate of the *Tridacna* XB10 and the TC activities during the summer-autumn of 2012. (a) 3-hour resolution wind speed from the Shanhu Island weather station during the summer-autumn of 2012. (b) TCs that have significant impacts on sampling site during the summer-autumn of 2012. The larger the circle represents the stronger the TC and the deeper the red represents the closer the TC to the sampling site (*SI Appendix, Method S1*). (c) The LTI time series during the summer-autumn of 2012. (d and e) Daily growth rate (DGR-XB10) and daily growth rate variance (DGRV-XB10) profiles during the summer-autumn of 2012. The purple shades indicated one to one match between the decrease of the daily growth rate by at least 15% and TCs. The olive shades indicated the decrease of the daily growth rate by at least 15% without corresponding TCs.

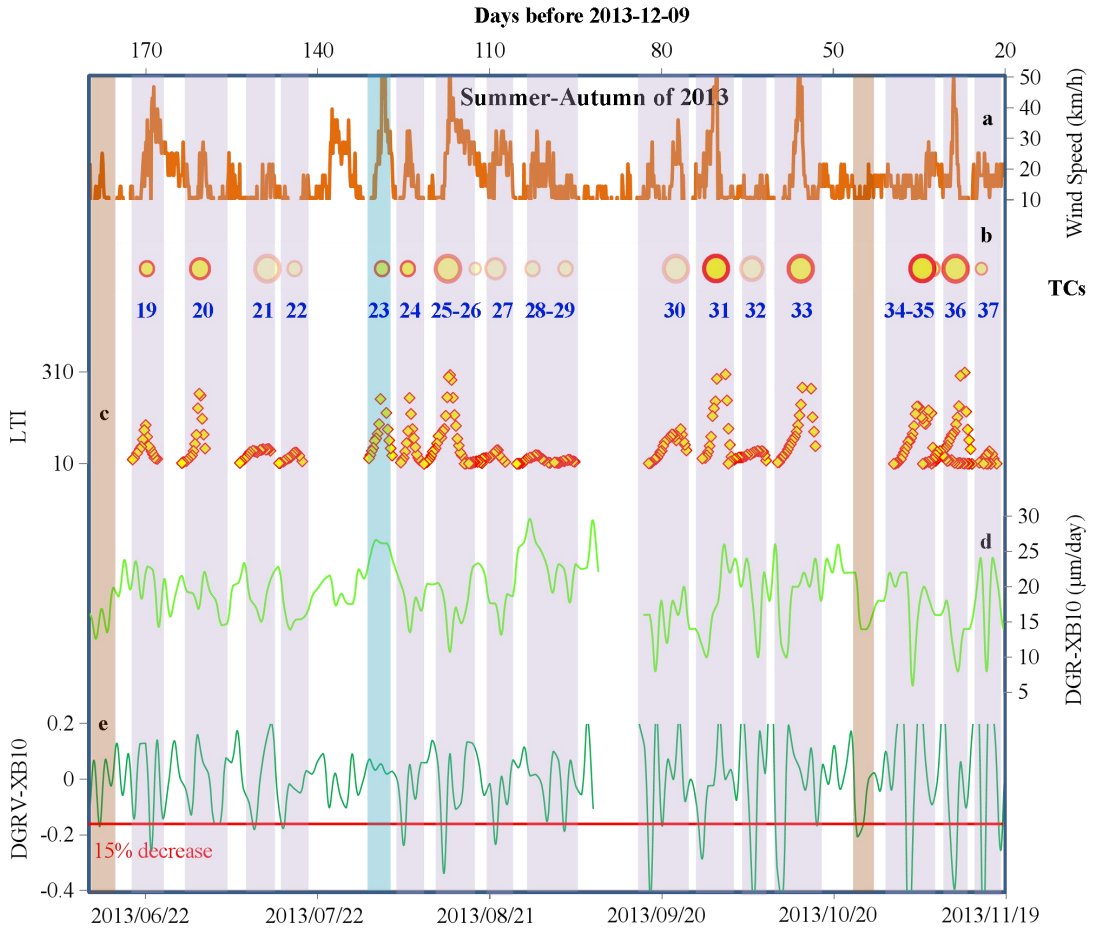

Figure S8-B The matches between the decreased daily growth rate of the *Tridacna* XB10 and the TC activities during the summer-autumn of 2013. (a) 3-hour resolution wind speed from the Shanhu Island weather station during the summer-autumn of 2013. (b) TCs that have significant impacts on sampling site during the summer-autumn of 2013. The larger the circle represents the stronger the TC and the deeper the red represents the closer the TC to the sampling site (*SI Appendix, Method S1*). (c) The LTI time series during the summer-autumn of 2013. (d and e) Daily growth rate (DGR-XB10) and daily growth rate variance (DGRV-XB10) profiles during the summer-autumn of 2013. The purple shades indicated one to one match between the decrease of the daily growth rate by at least 15% and TCs. The blue shades indicated the TCs without corresponding decrease of the daily growth rate by at least 15% and the olive shades indicated the decrease of the daily growth rate by at least 15% without corresponding TCs.

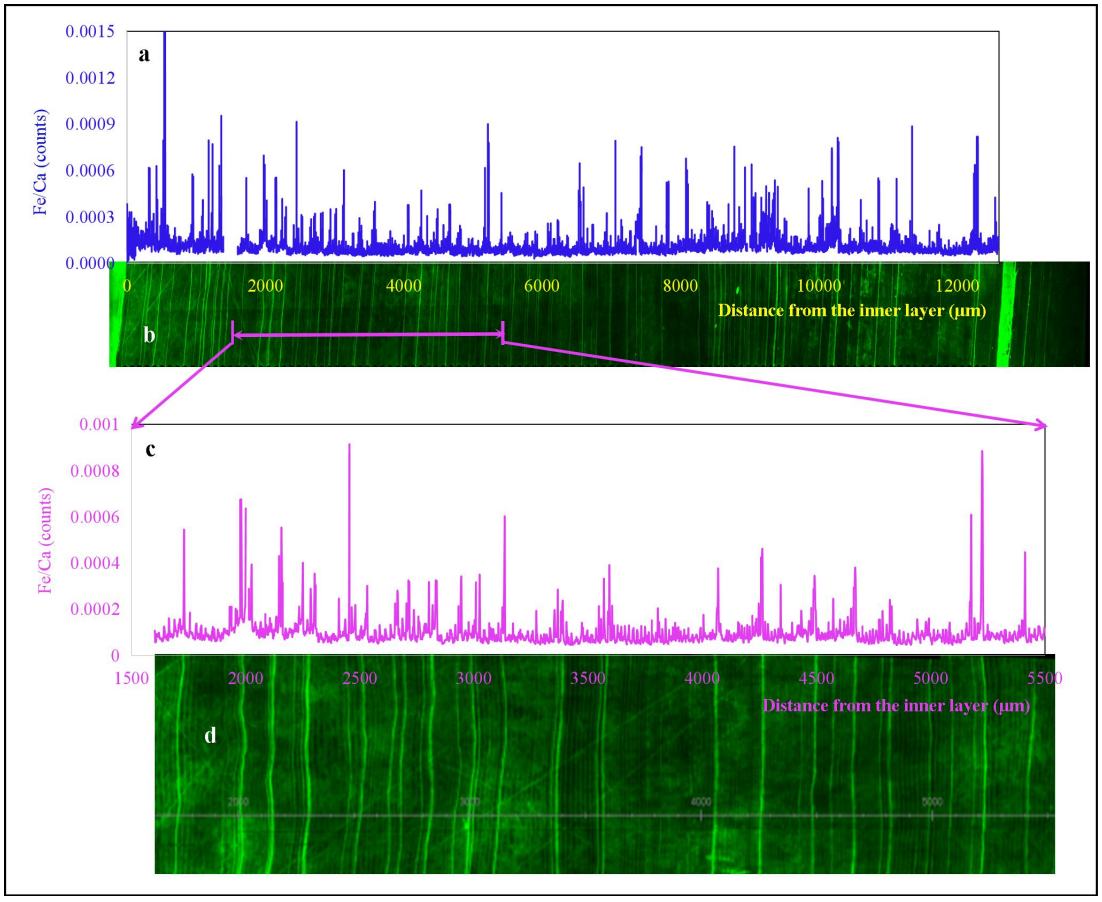

Figure S9 The matches between the abrupt enhanced fluorescence intensity of *Tridacna* XB10 and the pulsed peaks of Fe/Ca. (a) Fe/Ca ratios of XB10 determined by NanoSIMS during the 12.6 mm growth life. (b) Fluorescence intensity micro-image obtained by LSCM. (c) Fe/Ca ratios of XB10 from 1500 μm to 5500 μm. (d) Fluorescence intensity from 1500 μm to 5500 μm. The Fe/Ca pulsed peaks are highly correlated with the abrupt enhanced fluorescence intensity. The increased vertical mixing during the TC activity would bring the nutrient-enriched subsurface water to the surface, increasing the Fe and nutrient concentration in surface seawater and resulting in high Fe/Ca ratio and strong fluorescence intensity (caused by a phytoplankton bloom associated with higher organic matter in the surface seawater) in the carbonate shell of *Tridacna*.

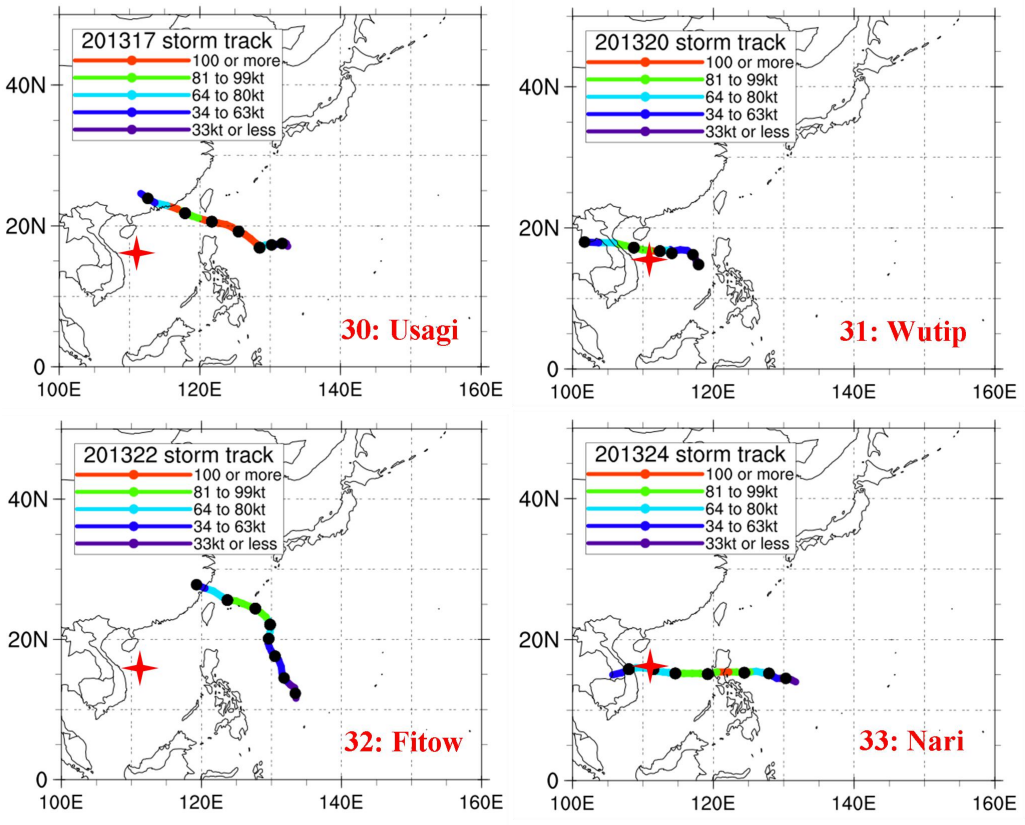
201317 storm track
100 or more
81 to 99kt
64 to 80kt
34 to 63kt
33kt or less
30: Usagi
201320 storm track
31: Wutip
201322 storm track
32: Fitow
201324 storm track
33: Nari
40N
20N
0
100E
120E
140E
160E

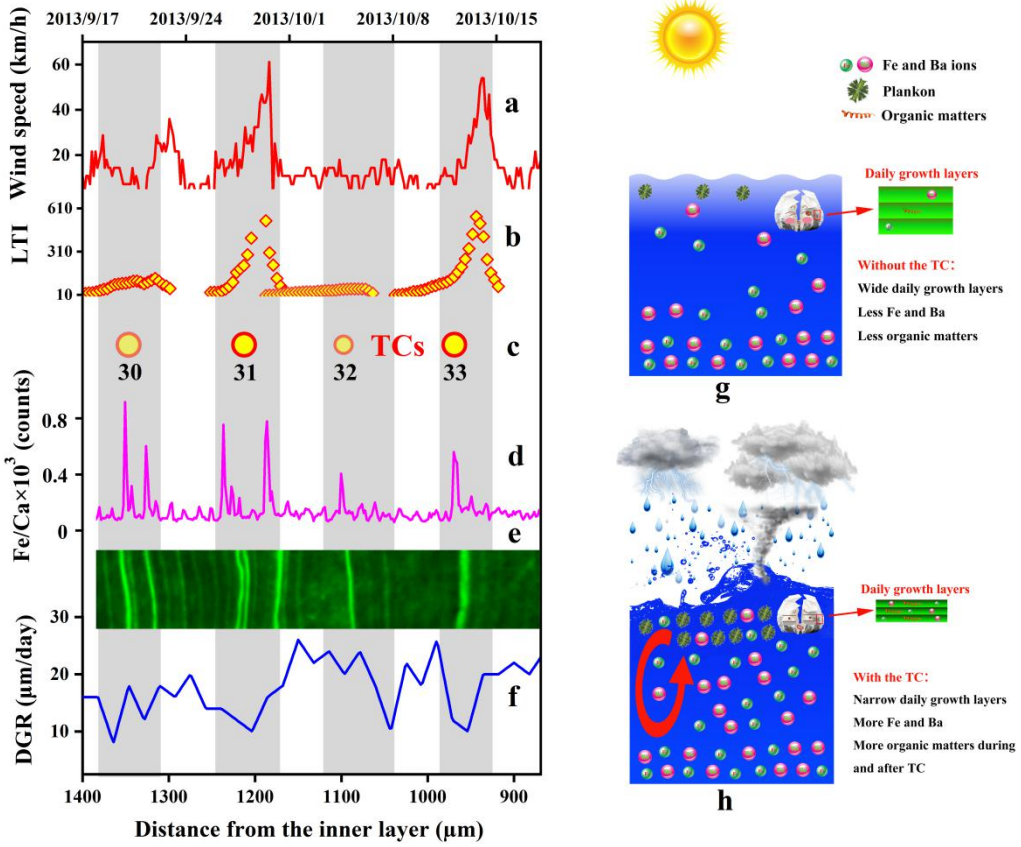
2013/9/17
2013/9/24
2013/10/1
2013/10/8
2013/10/15
Wind speed (km/h)
LTI
TCs
30
31
32
33
Fe/Ca×10³ (counts)
DGR (μm/day)
Distance from the inner layer (μm)
a
b
c
d
e
f
Fe and Ba ions
Plankon
Organic matters
Daily growth layers
Without the TC:
Wide daily growth layers
Less Fe and Ba
Less organic matters
g
With the TC:
Narrow daily growth layers
More Fe and Ba
More organic matters during
and after TC
h

Figure S10 The impacts of TCs on the proxy records of *Tridacna* shell. Top: The trajectories of four tropical cyclones (Number 30, 31, 32 and 33) during the autumn of 2013 (2013/09/17 to 2013/10/20). The red star indicates the sampling site North Reef of this study. Bottom: (a) 3-hour resolution wind speed of sampling site. (b) The LTI time series. (c) The TCs that have significant impacts on regional climate. (d) Fe/Ca profile of XB10. (e) Fluorescence intensity of the XB10. (f) Daily growth rate profile of the *Tridacna derasa* XB10. The gray shades indicate the four TCs. (g and h) Sketch map for the impacts of TC on *Tridacna* shell. (g) State without TC activity. (h) State with the TC activity. During the TC activity, the growth rate of *Tridacna* shell would decrease abruptly due to the strong wind, big sea waves, heavy rainfall and less insolation. The enhanced Ekman pumping and vertical mixing during the TC would bring the nutrient-enriched subsurface water to the surface and then increase the Fe, Ba and nutrient concentrations in surface seawater, resulting in high Fe/Ca ratio and strong fluorescence intensity in *Tridacna* shell associated with phytoplankton bloom and high dissolved organic matters after the TC.

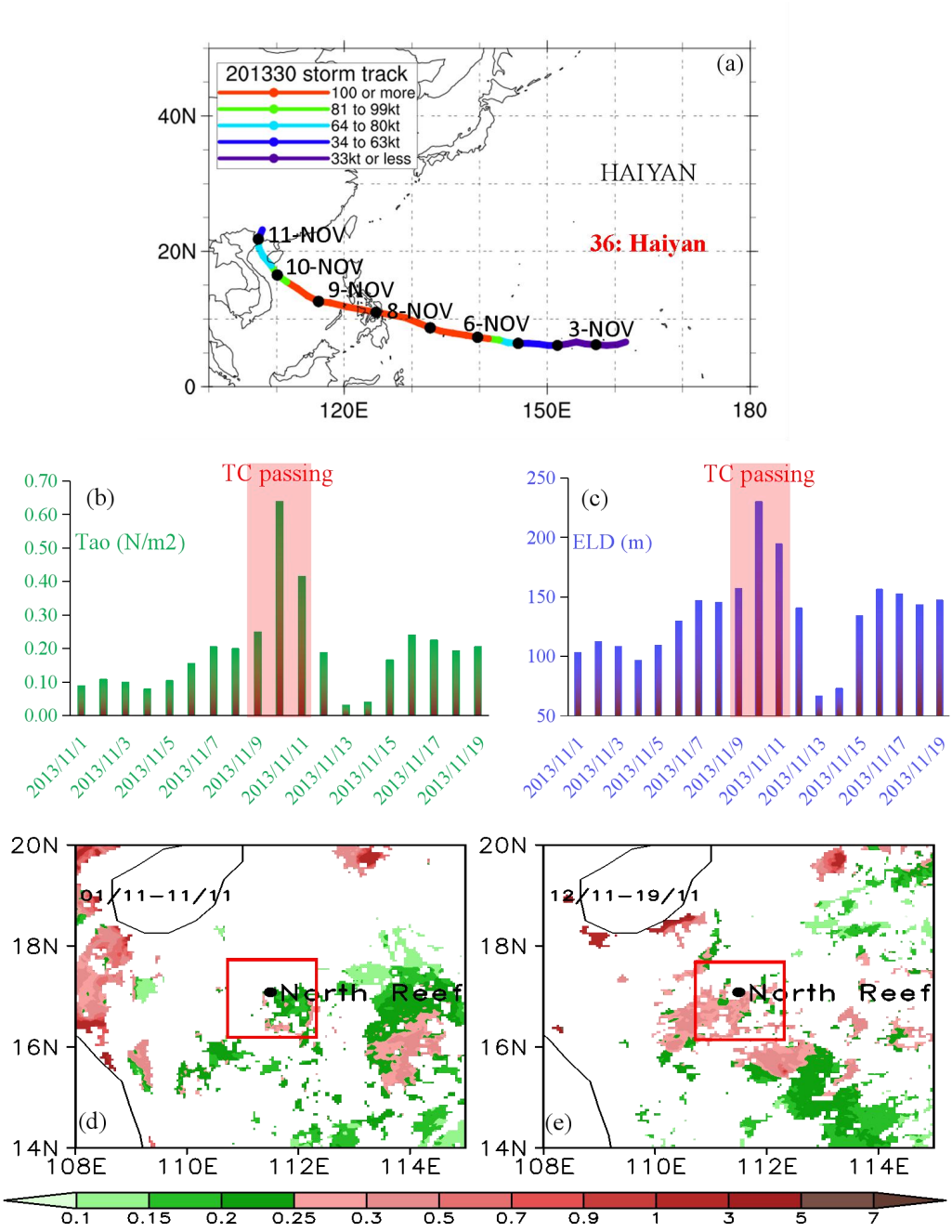

Figure S11 Impacts of tropical cyclones on local weather condition, ocean physical and biological processes. (a) Trajectory of tropical cyclone HAIYAN in November of 2013. (b) The wind-stress (Tao) around North Reef before, during and after the passing of HAIYAN. (c) The maximum occurrence depth of Ekman pumping (ELD) around North Reef before, during and after the passing of HAIYAN. (d and e) Sea surface chlorophyll a concentration around North Reef before and after the passing of HAIYAN (Shading, Unit: ug/m^3) based on multi-satellite observations (data source in *SI Appendix, Method S1*). The increased wind-stress and Ekman pumping during the TC activity would upwell the nutrient-enriched subsurface water to the surface, increasing the Fe and nutrient concentration in surface seawater and resulting in a chlorophyll a bloom (e) i.e., phytoplankton bloom, in sea surface after

the TC activity. The 3-day averaged sea surface wind vectors at 10 m above the sea with spatial resolution of 25 km, which were derived from satellite data, are produced by Remote Sensing Systems (www.remss.com). The wind-stress (Tao) and Ekman pumping layer depth (ELD) can be calculated as follows: According to previous studies(*18-20*), Tao=$\rho_a C_D \ \overline{U}_{10} \ \overline{U}_{10}$, where ρ_a and $\overline{U}_{10}$ are the air density and wind vector at 10 m above the sea, and $C_D = (0.73 + 0.069U_{10}) \times 10^{-3}$ is the drag coefficient. Moreover, the Ekman layer depth (ELD) is the depth where Ekman pumping exists, whose value does not only represent the physics of SSW but also indicates the intensity of subsurface ocean Ekman pumping process at fixed latitude, which can be computed from: $\mathrm{ELD} = \frac{7.6}{\sqrt{\sin\varphi}}\mathrm{U}_{10}$, where U_{10} is the wind speed at 10 m above the sea, and φ is the absolute value of the latitude(*20*).

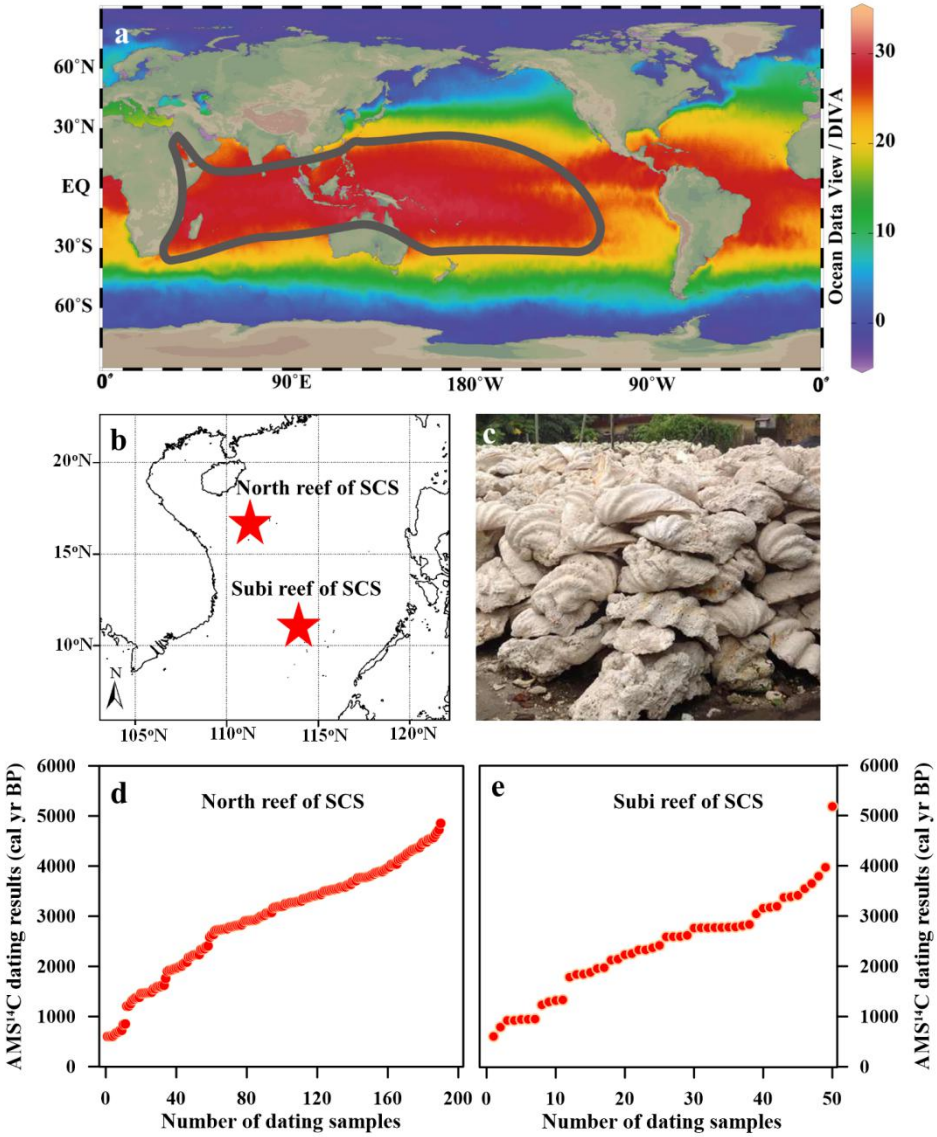

Figure S12 Sub-fossil *Tridacna* shells from the Indo-Pacific region. *Tridacna* are widely distributed in the coral reef systems of the Indo-Pacific tropical oceans. *Tridacna* shells are sessile during their whole life and generally deposit in-situ after death. Thus, by collecting the sub-fossil shells from top to bottom in a coral reef, we can theoretically obtain a continuous "sedimentary sequences" of *Tridacna* shells across different periods. Based on this notion, more than 1000 sub-fossil *Tridacna* shells were collected from two coral reefs of SCS, the North Reef and Subi Reef. 200 sub-fossil *Tridacna* shells from North Reef and 50 shells from Subi Reef were selected and AMS dating results showed that the samples from two coral reefs basically provide continuous coverage over the past 5000 years. These sub-fossil samples can be used to investigate the past WEEs variations in different climate settings during the mid-late Holocene. (a) The gray contour indicates the modern geographical distribution of *Tridacna*. (b and c) More than 1000 sub-fossil *Tridacna* shells were collected from North Reef and Subi Reef of SCS. (d and e) AMS dating results of the sub-fossil *Tridacna* shells from North Reef and Subi Reef.

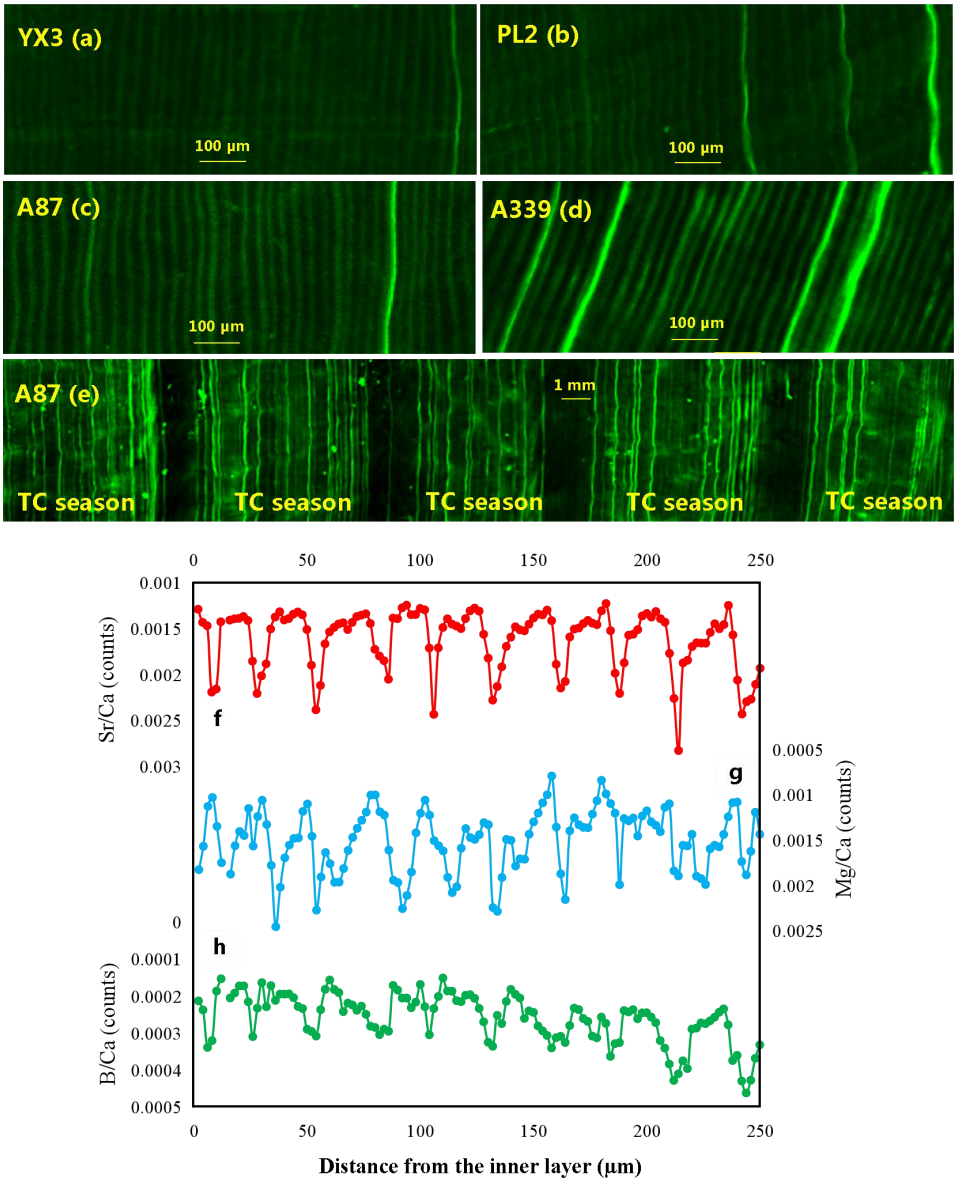

Figure S13 Fluorescence intensity micro-images and ultra-high resolution elements/Ca ratios obtained by LSCM and NanoSIMS in the other modern and fossil *Tridacna* shells collected from different locations in the western Pacific. Daily growth layers obtained by LSCM for modern *Tridacna derasa* shell YX3 from northern SCS (a), modern *Tridacna gigas* shell PL2 from Palau Islands (b) and fossil *Tridacna gigas* shells A87 and A339 from northern SCS (c and d). AMS dating results suggested that the fossil shells A87 and A339 lived around 3597 (± 39) and 2607 (± 31) years before present, respectively. 5-year long fluorescence intensity micro-image of A87 (e) presented five clear TC seasons and each TC season had many strikingly bright stripes probably caused by TC occurrences. (Below panel) Sr/Ca (a), Mg/Ca (b) and B/Ca (c) ratios of fossil *Tridacna gigas* shell A339 obtained by NanoSIMS. The clearly daily growth layers, daily Sr/Ca cycles and strikingly bright fluorescence stripes of these *Tridacna* shells indicate that the LSCM and NanoSIMS technologies are reliable in *Tridacna* paleoweather research.

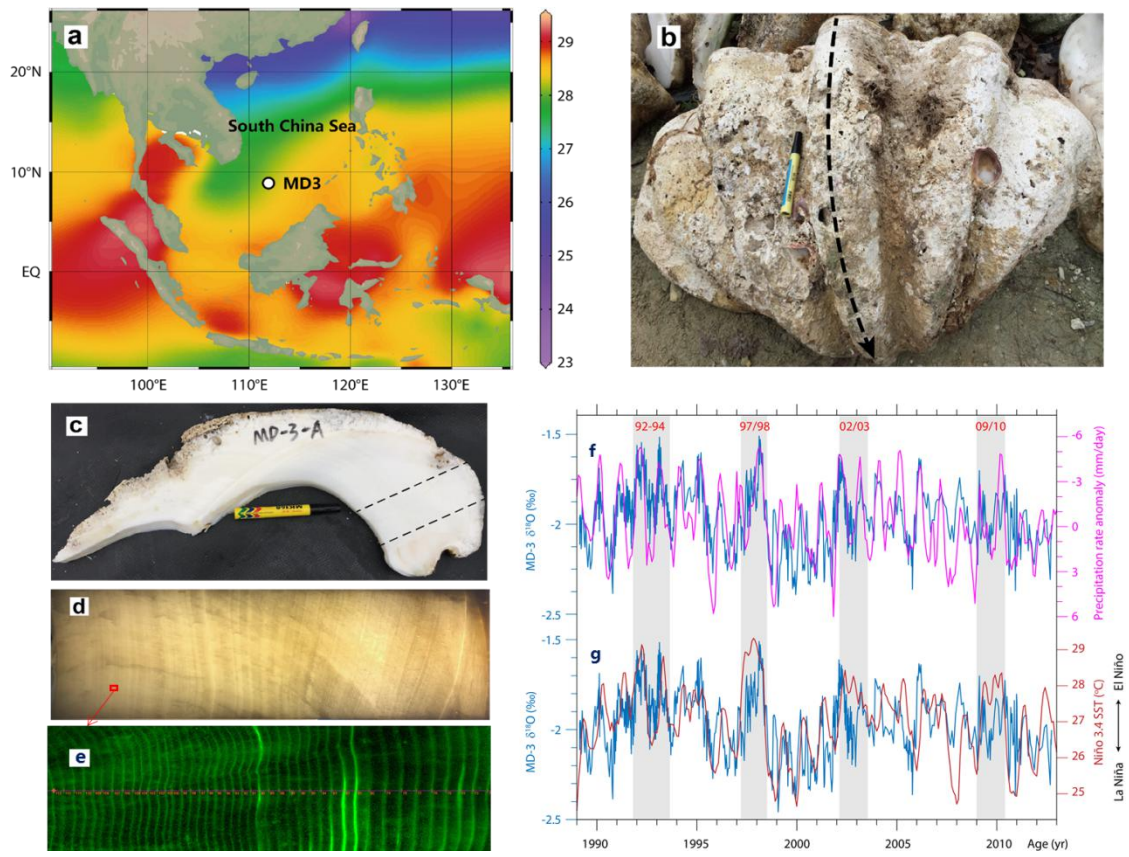

Figure S14 The daily growth bands in *Tridacna* shell from southern SCS. (a) The living *Tridacna gigas* shell MD-3 was collected in February 2013 from the Yongshu Reef (9º13'N, 112º54'E) of Nansha Islands, SCS. (b) Photograph of *T. gigas* bivalve MD-3 shell. (c) Cross section of the MD-3 shell. (d) Sub-sectioned shell slab from the cross section. (e) Micrographs of daily growth bands of the MD3 derived from the LSCM. (f and g) ^{18}O time series of MD3 and its relationship with the local precipitation anomaly and Niño 3.4 SST. To verify whether there is a daily growth layer deletion, a living *Tridacna gigas* shell named MD3 was collected from the Yongshu Reef of the South China Sea and the daily growth layers were counted. The $\delta^{18}O$ annual cycles, annual growth bands and the correlation between $\delta^{18}O$ and Niño 3.4 SST suggested that this shell has a life-span of 23.5 to 24 years. The counted total number of daily growth layers is 8649, with an average of 360 to 368 layers per year, indicating that there are almost no daily growth layers missing in the whole life process of the *Tridacna* shell MD3.

References

1. J. Rosewater, The family Tridacnidae in the Indo-Pacific. *Indo-Pacific Mollusca* **1**, 347-396 (1965).
2. K. Bonham, Growth Rate of Giant Clam Tridacna gigas at Bikini Atoll as Revealed by Radioautography. *Science* **149**, 300-302 (1965).
3. Y. Sano *et al.*, Past daily light cycle recorded in the strontium/calcium ratios of giant clam shells. *Nature Communications* **3**, 761 (2012).
4. H. Yan, D. Shao, Y. Wang, L. Sun, Sr/Ca profile of long-lived *Tridacna gigas* bivalves from South China Sea: a new high-resolution SST proxy. *Geochimica Et Cosmochimica Acta* **112**, 52-65 (2013).
5. V. Warter, W. Müller, Daily growth and tidal rhythms in Miocene and modern giant clams revealed via ultra-high resolution LA-ICPMS analysis—A novel methodological approach towards improved sclerochemistry. *Palaeogeography, Palaeoclimatology, Palaeoecology* **465**, 362-375 (2017).
6. V. Warter, J. Erez, W. Müller, Environmental and physiological controls on daily trace element incorporation in Tridacna crocea from combined laboratory culturing and ultra-high resolution LA-ICP-MS analysis. *Palaeogeography, Palaeoclimatology, Palaeoecology* **496**, 32-47 (2018).
7. M. Elliot *et al.*, Profiles of trace elements and stable isotopes derived from giant long-lived *Tridacna gigas* bivalves: Potential applications in paleoclimate studies. *Palaeogeogr Palaeocl* **280**, 132-142 (2009).
8. H. Yan, W. Soon, Y. Wang, A composite sea surface temperature record of the northern South China Sea for the past 2,500 years: A unique look into seasonality and seasonal climate changes during warm and cold periods. *Earth-Science Reviews* **141**, 122-135 (2015).
9. E. Vander Putten, F. Dehairs, E. Keppens, W. Baeyens, High resolution distribution of trace elements in the calcite shell layer of modern Mytilus edulis: environmental and biological controls. *Geochimica et Cosmochimica Acta* **64**, 997-1011 (2000).
10. T. Komagoe, T. Watanabe, K. Shirai, A. Yamazaki, M. Uematu, Geochemical and microstructural signals in giant clam Tridacna maxima recorded typhoon events at Okinotori Island, Japan. *Journal of Geophysical Research: Biogeosciences* **123**, 1460-1474 (2018).
11. A. Yamazaki *et al.*, Seasonal variations in the nitrogen isotope composition of Okinotori coral in the tropical western Pacific: A new proxy for marine nitrate dynamics. *Journal of Geophysical Research: Biogeosciences* **116**, 5343-5345 (2011).
12. I. I. Lin *et al.*, New evidence for enhanced primary production triggered by tropical cyclone. *Geophysical Research Letters* **30**, 1718 (2003).
13. S. Shang, L. Li, F. Sun, J. Wu, S. Shang, Changes of temperature and bio-optical properties in the South China Sea in response to Typhoon Lingling, 2001. *Geophysical Research Letters* **35**, L10602 (2008).
14. L. Sun, Y. J. Yang, T. Xian, Z. Lu, Y. F. Fu, Strong enhancement of chlorophyll a concentration by a weak typhoon. *Marine Ecology-Progress Series* **404**, 39-50 (2010).
15. P. Isdale, Fluorescent bands in massive corals record centuries of coastal rainfall. *Nature* **310**, 578-579 (1984).
16. P. J. Isdale, B. J. Stewart, K. S. Tickle, J. M. Lough, Palaeohydrological variation in a tropical

river catchment: a reconstruction using fluorescent bands in corals of the Great Barrier Reef, Australia. *Holocene* **8**, 1-8 (1998).

17. J. M. Lough, Great Barrier Reef coral luminescence reveals rainfall variability over northeastern Australia since the 17th century. *Paleoceanography* **26**, PA2201 (2011).
18. J. Garratt, Review of drag coefficients over oceans and continents. *Monthly weather review* **105**, 915-929 (1977).
19. M. D. Powell, P. J. Vickery, T. Reinhold, Reduced drag coefficient for high wind speeds in tropical cyclones. *Nature* **422**, 279-283 (2003).
20. Y.-J. Yang *et al.*, Impacts of the binary typhoons on upper ocean environments in November 2007. *Journal of Applied Remote Sensing* **6**, 063583 (2012).